Short Association Fibre Tractography

Dmitri Shastin[a,b,c,*], Sila Genc[a], Greg D. Parker[a], Kristin Koller[a], Chantal M.W. Tax[a,d], John Evans[a], Khalid Hamandi[a,c,e], William P. Gray[a,b,c], Derek K. Jones[a,c], Maxime Chamberland[a,f]

[a] *Cardiff University Brain Research Imaging Centre (CUBRIC), Cardiff University, Cardiff, United Kingdom*
[b] *Department of Neurosurgery, University Hospital of Wales, Cardiff, United Kingdom*
[c] *BRAIN Biomedical Research Unit, Health & Care Research Wales, Cardiff, United Kingdom*
[d] *Image Sciences Institute, University Medical Center Utrecht, Utrecht, Netherlands*
[e] *Department of Neurology, University Hospital of Wales, Cardiff, United Kingdom*
[f] *Donders Institute for Brain, Cognition and Behaviour, Radboud University, Nijmegen, Netherlands*

Abstract

Through advancing the existing and introducing novel methodological developments in streamlines tractography, this work proposes an approach that is meant to specifically interrogate an important yet relatively understudied population of the human white matter - the short association fibres. By marrying tractography with surface representation of the cortex, the framework: (1) ensures a greater cortical surface coverage through spreading streamline seeds more uniformly; (2) relies on precise filtering mechanics which are particularly important when dealing with small, morphologically complex structures; (3) allows to make use of surface-based registration for dataset comparisons which can be superior in the vicinity of the cortex. The indexation

*Corresponding author. Address: CUBRIC, Maindy Rd, Cardiff, United Kingdom, CF24 4HQ

Email address: sastind@cardiff.ac.uk (Dmitri Shastin)

of surface vertices at each streamline end enables direct interfacing between streamlines and the cortical surface without dependence on the voxel grid. Short association fibre tractograms generated using recent test-retest data from our institution are carefully characterised and measures of consistency using streamline-, voxel-, surface- and network-wise comparisons calculated.

Keywords: Short association fibers, U-fibers, superficial white matter, tractography, surface, consistency

---

1. Introduction

Functional integration of the brain subunits is mediated in part by the white matter (Neubert et al. (2010)), which comprises a vast network of connections between neuronal populations and has been shown to exhibit change in response to physiological processes (Scholz et al. (2009); Hihara et al. (2006); Dubois et al. (2014); de Groot et al. (2015); Slater et al. (2019)) and disease (Mito et al. (2018); Datta et al. (2017); de Schipper et al. (2019)). The white matter is typically divided into projection, commissural and association fibres. It is estimated that the association fibres dominate the white matter (Schüz and Braitenberg (2002)), connecting the cortical areas within hemispheres. They are in turn subdivided into long and short range (local) fibre, sometimes distinguishing neighbourhood association fibres as well (Schmahmann and Pandya (2006)). The long-range fibres course in the depth of the white matter, connecting distant areas of the hemisphere and forming distinct bundles that have largely consistent anatomy across individuals. Conversely, the short association fibres (SAF) connect adjacent cortical areas. Their most superficial component is often referred to as the U-shaped fibres and described as a thin band that runs immediately beneath the sixth layer of the cortex (Schmahmann and Pandya (2006)) encompassing a single gyrus or sulcus (Schüz and Braitenberg (2002)). It is established that neighbouring cortical areas exhibit the strongest structural connectivity (Markov et al. (2014)). Further, it is estimated that only $\sim 10\%$ of the cortico-cortical connections belong to the long fascicles, with the volume of the U-shaped fibres possibly as much as $\sim 60\%$ of the total white matter volume (Schüz and Braitenberg (2002)). It is remarkable therefore that in the neuroimaging

literature SAF have only started to gain more attention recently (Ouyang et al. (2017)).

Abbreviation	**Meaning/Interpretation**
ACT	Anatomically-constrained tractography
CVB	Between-subject coefficient of variation
CVW	Within-subject coefficient of variation
DKT	Desikan-Killiany parcellation
dMRI	Diffusion magnetic resonance imaging
DSI	Diffusion spectrum imaging
DTI	Diffusion tensor imaging
FA	Fractional anisotropy
FOD	Fibre orientation distribution
FWHM	Full-width half-maximum
GG	Grey-grey filter
GMWMI	Grey matter - white matter interface
GWG	Grey-white-grey filter
HARDI	High angular resolution diffusion imaging
HCP-MMP1	Human Connectome Project multi-modal parcellation
HH	Hemisphere-hemisphere filter
ICC	Intraclass correlation coefficient
LCHT	Local cortical half-thickness
MCC	Mid-cortical coordinate
PSM	Pial surface mesh
SAF	Short association fibres
TDI	Track density imaging
WSM	White surface mesh

Table 1: Table of abbreviations

Diffusion MRI (dMRI) is the preferred method for studying structural properties and connectivity of white matter pathways *in vivo*. Its sensitivity to the random microscopic motion of water molecules (Stejskal and Tanner (1965)) enables judgement to be made regarding the local directional architecture (Dell'Acqua and Tournier (2017)) and microstructural properties

(Assaf et al. (2019)) of the fibers. In the past few years, a number of dMRI-based studies have shown that SAF are affected by age and sex (Phillips et al. (2013)) as well as pathology including autism (d'Albis et al. (2018)), schizophrenia (Phillips et al. (2011), encephalitis (Phillips et al. (2018)) and epilepsy (O'Halloran et al. (2017); Liu et al. (2016); Govindan et al. (2013)), among others. dMRI methods used to study SAF can be broadly divided into those that do not use tractography and those that do. The former typically sample measures of microstructure in the superficial white matter as defined by regions of interest (Nazeri et al. (2013)) or uniformly along the cortical surface (Phillips et al. (2013, 2018, 2011); Liu et al. (2016)). This approach avoids any biases of tractography and can be less sensitive to the differences in cortical folding through the use of surface registration (Fischl et al. (1999)) but it does not discriminate between SAF and the superficial component of the long-range connections. On the other hand, tractography-based methods capitalise on local fibre orientation modelling which allows reconstruction of streamlines providing information about white matter morphology (Mori and Van Zijl (2002)). Numerous challenges, such as the inability to resolve multiple fibre directions in regions with complex fibre configurations, can create ambiguity and lead to a high number of false positive and false negative results during streamline generation (Maier-Hein et al. (2017)). Recent advances in image acquisition (Jones et al. (2018)) and processing as well as development of advanced fibre orientation estimation (Tournier et al. (2007); Dhollander et al. (2016); Jeurissen et al. (2014)) and streamline integration and filtering algorithms (Smith et al. (2012); Daducci et al. (2015); Smith et al. (2015)) have improved the quality of tractography. Despite this, avail-

able tools are typically used to study whole-brain tractograms or focus on the deep white matter bundles that show consistent organisation across individuals and thus the performance of these tools for investigating SAF remains uncertain.

2. Challenges in SAF reconstruction

2.1. Tractogram generation

The study of SAF is confounded by a number of anatomical considerations and methodological limitations (for an overview, see Guevara et al. (2020); Jeurissen et al. (2017); Rheault et al. (2020); Reveley et al. (2015)) which span initial tractogram generation, SAF-specific filtering and analysis. The tractogram generation step faces the challenges of partial volume effects (due to the proximity of SAF to cortex and CSF spaces) and complex local anatomy with multiple regions of crossing, bending, kissing, and fanning fibres. The subcortical location makes SAF potentially more sensitive to the so-called "gyral bias" - the phenomenon in tractography where many more streamlines terminate in the gyral crowns as opposed to the sulcal fundi (Li et al. (2010); Nie et al. (2011); Chen et al. (2012)). It remains unclear just how much of this effect is explained by methodological shortcomings (and can be improved) rather than underlying anatomy (see Van Essen et al. (2014) for a detailed discussion of the subject). Specifically in the context of U-shaped fibers, the gyral bias has been demonstrated even when state-of-the-art acquisition and tractography were used (Movahedian Attar et al. (2020)). Yet, capturing finer anatomical detail of SAF is important due to their short length and complex morphology.

2.2. Tractogram filtering

From the filtering perspective, SAF may be defined locally based on manual dissections or functional MRI signal-derived cortical regions of interest (Movahedian Attar et al. (2020)), whilst for globally (brain-wise) defined SAF, the filtering criteria typically involve size, shape and/or cortical parcellation. Despite the existence of studies examining the histopathology of SAF in isolated brain regions, the absence of a detailed anatomical knowledge regarding the distribution and consistency of SAF on a whole-brain level or even a universally accepted definition (Ouyang et al. (2017)) complicates development and validation of non-invasive methods dedicated to the study of this subset of the white matter. For instance, the size definition of SAF (or U-shaped fibres) varies across sources. Some authors have focused on the relatively long streamlines of 20-80 mm (Guevara et al. (2017); Kai and Khan (2019)) or more (Román et al. (2017)), mainly concerning the bundles connecting neighbouring gyri; while others (Song et al. (2014); Movahedian Attar et al. (2020)) included the smaller range of 3-30 mm based on the classification by Schüz and Braitenberg (2002). Next, although using streamline similarity measures (typically shape and distance metrics) as filtering criteria (Román et al. (2017); O'Halloran et al. (2017); Kai and Khan (2019)) may appear appealing, this may lead to exclusion of otherwise valid streamlines as SAF have been demonstrated to exhibit complex, diverse morphology (Movahedian Attar et al. (2020)) and varying spatial overlap (Zhang et al. (2010)); this is particularly true for shorter (<35 mm) streamlines (Román et al. (2017)). The use of cortical parcellations (division of the cortical mantle into discrete areas) can carry uncertainties of its own. The choice of parcellation

scheme, termination criteria during tracking, and the way streamlines are associated with individual parcels all influence the result (Yeh et al. (2019)). The use of larger parcels and discrete borders may not be particularly well-suited for studying SAF as both ends of many streamlines will terminate in the same cortical parcel leading to rejection; parcellation may also impose artificial boundaries that make little physiological sense.

2.3. Tractogram comparison

Group-wise analysis of SAF is challenged by inter-subject variations in cortical folding (Rademacher (2002)). Even the sulci known to exhibit more anatomical consistency across individuals (such as those corresponding to the primary somatosensory areas (Rademacher (2002)) demonstrate individual morphological differences up to 1-2 cm in a common reference frame (Steinmetz et al. (1989)). The trajectories of short (up to 40 mm) superficial streamlines appear to be strongly influenced by the gyral pattern (Bajada et al. (2019)). Taken together, one should expect low consistency when comparing SAF tractograms composed of shorter streamlines between individuals based on their shape or spatial distribution alone. Connectome-based comparisons using cortical parcellations are possible yet again they face the same challenges as described above.

Our proposed methodological framework overcomes some of the limitations that are specific to tractography of SAF (as defined in Schüz and Braitenberg (2002)) by incorporating a mesh representation of the cortical surface into the seeding and filtering steps and by introducing simple, anatomy-driven filtering criteria. This produces clean and physiologically plausible tractograms of SAF without the need for manual dissection/pruning or ad-

ditional shape/parcellation-based criteria. Finally, we compare these tractograms within and between subjects to assess consistency of the results, including with an alternative method of SAF analysis that relies on projecting streamline metrics onto the surface in native space.

3. Material and methods

3.1. Workflow

3.1.1. Streamline generation

The overall workflow is summarised in Figure 1. Streamline seeding and filtering with voxel-based masks can lead to smaller regions being excluded or misrepresented due to the discrete nature of the voxel grid (**??**), hence surface-based filters were employed for this pipeline. The first step to such an approach is to ensure streamline seeds are distributed approximately evenly on the surface. The FreeSurfer (Fischl (2012)) white matter surface mesh (WSM) typically contains ∼1.5 vertices/mm^2 for a total of ∼250K vertices for both hemispheres (excluding the medial wall) and an average face area of 0.32 mm^2 (range: 0.07-0.7 mm^2, top and bottom 2% excluded) representing a reasonably dense and even spread; this can be further re-meshed if needed. Vertex coordinates in each hemisphere were transformed to dMRI space with ANTs (Avants et al. (2009)) using the inverse warp (see subsubsection 3.2.1) and concatenated into a single array used to initiate seeding with MRtrix 3.0 (Tournier et al. (2019)). MRtrix was modified such that it can read coordinates from the array and use them as seeds with equal weights during tractogram generation. Results were verified by visual inspection of the seed distribution on T1-weighted volumes co-registered to dMRI space and by

comparing the input and output seed coordinates (data not shown). Tracking was performed using the second-order integration probabilistic algorithm iFOD2 (Tournier et al. (2010)) due to the expected large number of fibre crossings and challenging morphology; probabilistic tracking has previously been demonstrated to result in improved gyral bias (Nie et al. (2011)) and greater spatial overlap of SAF (Guevara et al. (2020)). A total of 5 million seeding attempts from the given seeds were made per tractogram to ensure an adequate number of streamlines per vertex. An additional restriction on the maximum streamline length of 40 mm was used (to be consistent with the SAF definition of Schüz and Braitenberg (2002) but accounting for the fact that intracortical portions were later truncated, see section 3.1.2); other parameters were left as their default settings in the MRtrix implementation of iFOD2.

3.1.2. Streamline filtering

By definition, a streamline representing association fibres must satisfy the following criteria: (1) both ends terminate in the neocortex; (2) both ends terminate in the same hemisphere; (3) the streamline courses through the white matter. Three respective filters ensuring these three criteria were met were applied to the initial tractogram.

Grey-grey (GG) filter. To identify streamlines starting and ending in the neocortex, midcortical coordinates (MCC) were defined by averaging coordinates of the matching WSM and pial surface mesh (PSM) vertices. Next, local cortical half-thickness (LCHT) was defined as the Euclidean distance between the MCC and the corresponding WSM vertex to account for lo-

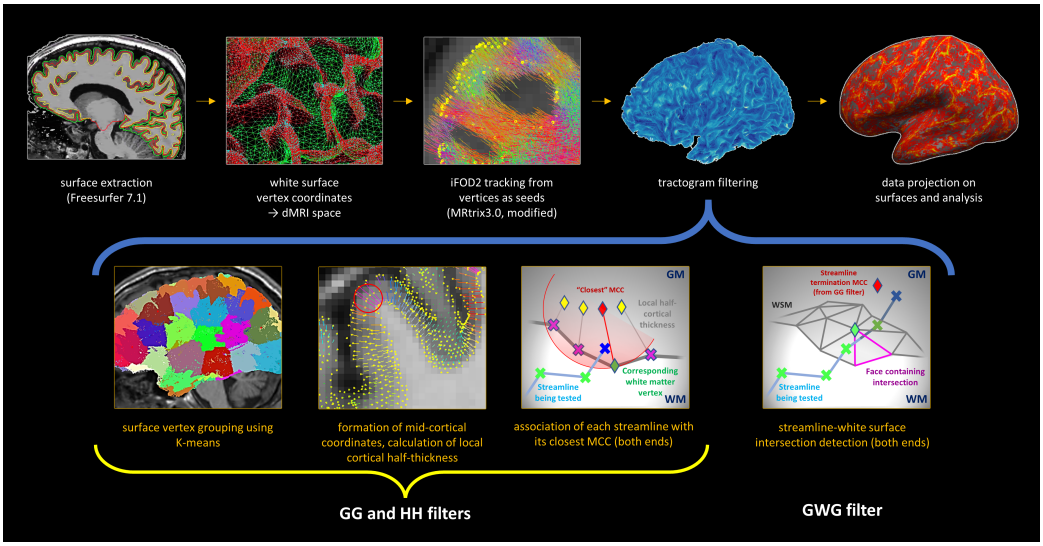

Figure 1: Pipeline summary. After seeding from white surface mesh (WSM) coordinates, tractograms were processed to ensure each streamline starts and ends in the neocortex (grey-grey filter) of the same hemisphere (hemisphere-hemisphere filter) and escapes into white matter along the way (grey-white-grey filter). The grey-grey filter functioned by finding the Closest midcortical coordinate (MCC, average of matching WS and pial coordinates) for each streamline end (with K-means clustering of MCCs for speed). A streamline end was considered in grey matter if it laid within the local cortical half-thickness of its MCC. Then, an iterative algorithm followed the streamline back searching for WSM intersection at which point the intracortical portion was truncated.

cal variation in cortical thickness. Both ends of each streamline in the initial tractogram were then evaluated for "intracortical position" by (1) identifying the closest MCC, (2) measuring the Euclidean distance to it, (3) comparing this distance to the LCHT measure of said MCC. The "intracortical position" was confirmed if the streamline terminated in a sphere centred on the MCC and with the radius LCHT (also see **??**).

To improve computational efficiency, all MCC were clustered with the K-

means algorithm using squared Euclidean distances (Arthur and Vassilvitskii (2006)); finding the centroid closest to a streamline end meant the closest MCC had only to be identified within the cluster of that centroid (see **??** for details).

Hemisphere-hemisphere (HH) filter. The original hemispheric membership (left or right) of all cortical vertices and thus MCC was known; the hemispheric allocation of each streamline end became apparent once its closest MCC was identified during GG filtering. This filter acted by only selecting streamlines whose both ends resided in the same hemisphere.

Grey-white-grey (GWG) filter. After ensuring all streamlines terminated intracortically, the last filter needed only to follow streamlines back and detect escape into white matter. Due to the possibility of this happening on a subvoxel scale, and because the exact point of intersection with WSM was of interest, filtering was performed with an *ad hoc* iterative algorithm (see **??** for details) instead of applying a simple white matter mask.

In short, the algorithm operated by selecting a WSM vertex and testing its faces for intersection with a streamline segment (straight line connecting two adjacent points). The first WSM vertex was selected to match the MCC of streamline termination, and the first streamline segment was the one containing the termination. Despite the MCC being the closest to the segment, its corresponding WSM vertex did not have to be. Hence, if no intersection was found, other vertices of the faces just tested were next considered and of those, the vertex closest to the streamline segment was chosen. The algorithm propagated along the surface moving closer and closer to the streamline segment as it kept selecting from adjacent vertices and testing

faces along the way for intersection until either: (1) an intersection was found; or (2) no vertex closer to the streamline segment was identified. In case of the latter, propagation along the streamline occurred instead and the next segment was interrogated in a similar fashion. The algorithm ran for each streamline until an intersection was found, or the whole streamline was examined. Such propagation, as opposed to simply testing faces of vertices closest to each streamline segment, was preferred because in some cases intersection occurred with faces of vertices that were not the closest. In addition to detecting escape into white matter, GWG filter allowed to register WSM vertices closest to the intersection (i.e., associate each end of each streamline with its WSM vertex); and truncate streamlines at that point if desired. In this work, GWG was applied to both streamline ends which were then truncated at WSM.

3.2. Framework evaluation

3.2.1. Data acquisition and pre-processing

Repeatability data from the MICRA study (Koller et al. (2020)) were used for framework evaluation. In short, after a written informed consent, brain MR data of six healthy adults (3 males and 3 females, age range 24-30) were obtained using an ultra-strong gradient (maximum amplitude 300 mT/m) 3T Connectom scanner (Siemens Healthcare, Erlangen, Germany) in Cardiff University Brain Research Imaging Centre, Cardiff, United Kingdom. The higher gradients resulted in higher signal-to-noise ratio per unit time for a given b-value, allowing for utilisation of higher b-values which are more sensitive to intra-axonal water displacement (Jones et al. (2018); Setsompop et al. (2013); Genc et al. (2020)). Each subject was imaged five times us-

ing the same protocol within a two-week period at approximately the same time of day. Only anatomical (T1-weighted) and diffusion (dMRI) data were utilised for the purposes of this study.

dMRI data (single-shot spin echo, echo planar, voxel size: $2\times2\times2$ mm^3; b-values of 200, 500, 1200, 2400, 4000, 6000 s/mm^2 in 20, 20, 30, 61, 61, 61 noncollinear directions, respectively, with thirteen interspersed b0 volumes; TR/TE 3000/59 ms - see Koller et al. (2020); Setsompop et al. (2012) for details) were corrected for slicewise intensity outliers (Sairanen et al. (2018)), signal drift (Vos et al. (2017)), Gibbs artifact (Kellner et al. (2016)), eddy current distortion and motion artifact (Andersson and Sotiropoulos (2016)), echo-planar image distortion (Andersson et al. (2003)), and gradient non-linearities (Glasser et al. (2013)). Pre-processed data were upsampled to 1x1x1 mm^3 (Dyrby et al. (2014)). Diffusion tensor estimation in each voxel was performed with nonlinear least squares. The fibre orientation distribution (FOD) (Tournier et al. (2007)) was derived using 3-tissue response function estimation (Dhollander et al. (2016)) and subsequent multi-shell multi-tissue constrained spherical decomposition (Jeurissen et al. (2014)) with harmonic fits up to the eighth order. The quality of the pre-processing steps as well as FOD distributions were visually confirmed for all subjects.

Anatomical data (Siemens MPRAGE1 sequence, voxel size: 1x1x1 mm^3, TR/TE 2300/2.81 ms) were run through the FreeSurfer 7.1 package (Fischl (2012)) which includes standard T1-weighted volume pre-processing steps. The longitudinal stream designed for repeated acquisitions was used (Reuter et al. (2012)). One subject lacked a T1-weighted volume for one of the sessions; instead, the within subject template (referred to as "base" in the

longitudinal stream) was used, resulting in a total of six "base" and twenty-nine final (referred to as "long") sets. The quality of produced surface meshes was visually inspected at every step and corrected where necessary as per the standard FreeSurfer protocol. dMRI-derived fractional anisotropy (FA) volumes were non-linearly registered to FreeSurfer T1-derived "brain" volumes using ANTs; coordinates of surface vertices were then brought into DWI space using the inverse transform and registration quality was visually confirmed in each case. An average subject was created for group analyses from the six "base" sets with FreeSurfer's *make_average_subject* command and used as a common space template for all "long" sets (surface co-registration done with *surfreg*).

3.2.2. Effects of surface seeding

A modified version of the established MRtrix ACT/GMWMI was executed on the same data to compare the effects of the two seeding methods on subsequent filtering. First, FreeSurfer's "aseg" volume was transformed to dMRI space using the already available registration and nearest neighbour interpolation (preserving segmentation labels). This acted as the input into MRtrix's FreeSurfer-based five-tissue-type (5TT) segmented tissue image generation algorithm (Smith et al. (2012)). The 5TT image was then manipulated such that the cerebellar cortex and the amygdala/hippocampus were excluded from the grey matter volume (matching the cortical areas used in surface seeding), while the deep nuclei as well as the ventricles were added to the white matter volume with their original volumes set to null. The manipulation effectively forced all streamlines to start and end at the neocortex. A grey matter-white matter interface (GMWMI) volume was generated and

seeding performed until the total number of streamlines for ACT/GMWMI matched the same number generated with surface seeding (see subsubsection 3.1.1); analogously, streamline length was confined to ≤ 40 mm. Streamlines were then GG-filtered such that only those with both ends within the cortex remained. HH and GWG filtering were not performed as they depend on the results of the GG filter and, when compared to the latter, reject far smaller number of streamlines. Streamline end-associated "intersection" MCC indices (as the output of GG) were used for surface-based analyses.

The effects of the two seeding methods were evaluated by comparing GG-filtered tractograms on the following characteristics: (1) number of streamlines surviving filtering; (2) cortical coverage (proportion of vertices with streamlines); (3) number of streamlines associated with each vertex; (4) proportion of "covered" surface representing gyri (estimated as proportion of streamline-linked surface vertices with a negative FreeSurfer "sulc" value).

3.2.3. Tractogram characteristics and assessment of consistency

The following complementary approaches were chosen to evaluate the generated SAF tractograms: (1) general streamline metrics; (2) volume-based track density imaging (TDI) maps (Calamante et al. (2010)); (3) surface-based projections of streamline metrics; (4) connectome-based graph theory metrics. The focus of these assessments was to provide a description of the tractograms and to test their consistency within and between subjects rather than producing inferences about the physiological properties of SAF themselves.

General streamline measures. SAF tractograms were assessed and compared using the following criteria: (1) streamline count; (2) mean streamline length; (3) mean streamline FA derived by sampling respective FA volumes along each streamline with MRtrix's *tcksample* command (mean FA across each streamline).

TDI maps. TDI maps for each session were generated with MRtrix's *tckmap* command. The maps were compared in average subject space by applying the previously obtained dMRI-to-T1 transform followed by a "base-to-average" transform (concatenated and performed in a single step using ANTs).

Surface-based analysis. Each streamline terminated at two WSM vertices (one per end) allowing streamline-related metrics to be recorded at these vertices in native space. This enabled the use of surface-based registration for comparisons, which due to the complexities of cortical folding, can be superior to volume-based registration for these superficial structures. The following metrics were thus recorded: (1) number of streamlines per vertex; (2) cortical coverage (binarised version of the former); (3) mean streamline length per vertex; (4) mean FA per streamline per vertex. The latter can be thought of as being conceptually similar to uniform sampling of FA (or, indeed, any scalar) along the surface, with the exception that the size and shape of the sampling kernel changed informed by the streamlines at the vertex being sampled, and the sampling occurred exceptionally in the white matter.

Results were saved in FreeSurfer "curv" format (**??**). Two types of analysis were performed: (1) using average values for all vertices of both hemispheres; (2) directly comparing surfaces on a per-vertex basis per hemisphere.

For the latter, corresponding "curv" files were stacked (*mris_preproc*) and smoothed (*mri_surf2surf*) at 5 mm full-width at half-maximum (FWHM). Smoothing is commonly used in neuroimaging to boost signal-to-noise ratio, alleviate registration misalignment, and improve normality of residuals. As per-vertex testing was not sensitive to between-vertex interactions, smoothing provided an alternate means to account for these interactions. For all surface-based analyses, only the cortical surface (excluding the "medial wall" label) was studied.

Graph theory metrics. The cortex was parcellated using FreeSurfer with two different atlases: (1) the Desikan-Killiany parcellation atlas (DKa) producing 31 regions per hemisphere; (2) the Human Connectome Project multi-modal parcellation (HCP-MMP1) producing 180 regions per hemisphere (Glasser et al. (2016); Mills (2016)). Weighted connectivity matrices were constructed for each hemisphere separately as they shared no connections. Edge weights were generated from streamline counts to evaluate tractogram consistency by determining which surface label the ends of each streamline belonged to (termination at WSM was recorded during filtering). The Brain Connectivity Toolbox (version: 2019-03-03, Rubinov and Sporns (2010)) was used to normalise connectivity matrix entries to [0,1] and remove self-connections. Next, network density (ρ) and weighted network metrics including network strength ($\mathrm{K^W}$), betweenness centrality ($\mathrm{B^W}$), characteristic path length ($\mathrm{L^W}$), global efficiency (E_G^W), local efficiency (E_L^W), and clustering coefficient ($\mathrm{C^W}$) were computed. For each node-wise network measure (i.e. $\mathrm{K^W}$, $\mathrm{B^W}$, $\mathrm{C^W}$, and E_L^W), the average over all nodes was used.

3.2.4. Statistical analysis

To compare surface seeding with ACT, a two-tailed paired sample t-test was used. In subsequent experiments, consistency of SAF tractograms was evaluated by examining metric reproducibility, between-subject variability and reliability. The former two were calculated using within (CV_W) and between (CV_B) subject coefficients of variation, respectively (Laguna et al. (2020)). Reliability of metrics was characterised using single measurement intraclass correlation coefficient for absolute agreement ICC(3,1) with subject effects modelled as random and session effects fixed (McGraw and Wong (1996)). The data were formulated with a linear mixed-effects model (Chen et al. (2018)). For voxel-based (TDI) and surface-based analysis, CV_W, CV_B and ICC were calculated at each voxel/vertex. All statistical analyses were performed in MATLAB 2015a.

3.3. Data/code availability statement

- Data: please refer to Koller et al. (2020) for access to the test-retest data.

- Code: the MATLAB code for filtering of SAF and interfacing with the surface will be made available shortly after publication at: *https://github.com/dmitrishastin/SAF*

4. Results

4.1. Effects of surface seeding

The distribution of successful seeds in relation to the WSM is illustrated in the top row of Figure 2. This demonstrates that surface seeding resulted

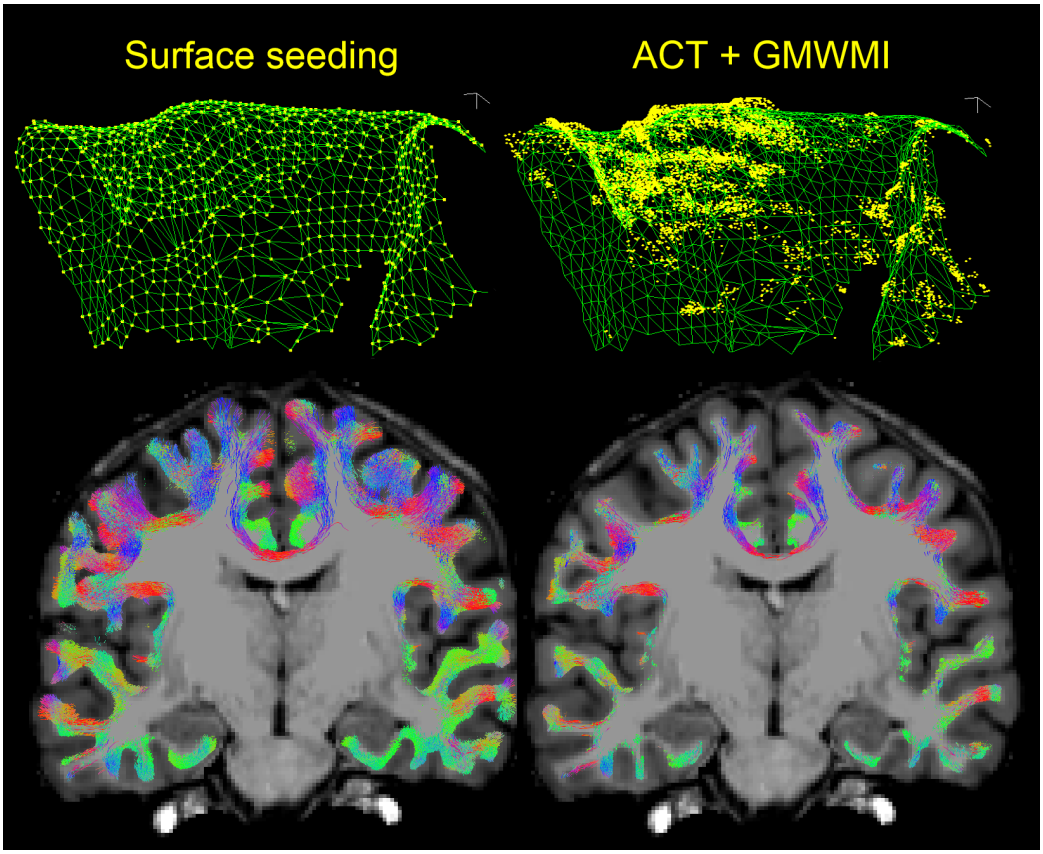

Figure 2: Tracking from the surface vertices (left) versus tracking using MRtrix ACT/GMWMI (right). Top row: distribution of seeding coordinates with each method (yellow) related to a section of the WSM (green), white lines show scale (1 mm) in three orthogonal directions. Surface seeding appears to achieve a more spatially uniform distribution and places seeds directly on the mesh (by definition). Bottom row: results of GG-filtering for both seeding methods (not truncated) overlaid on the T1-weighted volume (slice thickness: 1 mm). Surface-seeded streamlines extend into the grey matter, allowing to interface with the WSM.

in a smaller number of unique seeds (being confined to the WSM vertices only) yet provided a more consistent GMWMI coverage. The initial tractograms generated with the two methods looked very different (not shown)

because surface seeding does not use anatomical priors as streamline termination/rejection criteria; however, after GG filtering (in itself an anatomical prior) the distribution and course of streamlines in the white matter looked very similar (Figure 2, bottom row). Compared to ACT (Table 2), surface seeding resulted in a slightly larger number of streamlines surviving GG filtering ($p=0.006$). Importantly, 60% more MCCs were covered with streamlines ($p<0.001$) and each was associated with 240% more streamlines on average ($p<0.001$). This difference was likely influenced by the more consistent seed placement with surface seeding and the fact that with ACT, streamlines did not propagate into grey matter and occasionally even left a superficial rim of unfilled white matter (Figure 2). The latter would have prevented subsequent GG filtering from accepting some streamlines. Decreasing the FOD cut-off during tracking did not improve this result significantly. In contrast, surface seeding allowed tracking to propagate in both directions with non-white matter sections truncated later at the GWG filtering step. Additionally, the expected gyral bias was noticed with surface seeding as streamlines associated with more MCCs in gyri than in sulci whereas the reverse was true for ACT ($p<0.001$).

4.2. SAF tractograms

Tractograms appeared anatomically consistent and no manual pruning was required (Figure 3). On average, 20% of the original streamlines survived the filtering. Mean streamline length was 19.11 ± 0.16 mm after trimming the intracortical portions. The average FA per streamline was 0.31 ± 0.01. Tractograms covered 87.27 ± 1.78% of WSM vertices with 6.94 ± 1.10 streamlines per vertex. Mean streamline length and mean FA per vertex were similar to

	Surface Seeding		**ACT + GMWMI**[3]		
	Mean	**SD**	**Mean**	**SD**	**p**[4]
Number of streamlines generated	4.5M	0.1M	4.5M	0.1M	matched
Number of streamlines after GG filter[1]	1.1M	52K	1.0M	64K	0.006
Cortical coverage (%)[2]	88.36	2.14	55.72	1.08	0.000
Termination density (streamlines/vertex)[2]	18.39	2.55	7.68	1.06	0.000
Prevalence of gyri in the covered surface (%)[2]	52.77	0.65	47.95	0.58	0.000

[1] Streamlines starting and ending in the neocortex

[2] Calculated at MCC, averaged over all vertices of both hemispheres

[3] Using FreeSurfer algorithm, modified only to use the cortical ribbon

[4] Paired T-test (two-tailed) using within-subject averages

Table 2: Results of filtering after tracking from the surface vertices versus tracking using MRtrix ACT/GMWMI for the same initial number of streamlines. Seeding from the surface leads to more efficient subsequent filtering and a larger cortical coverage.

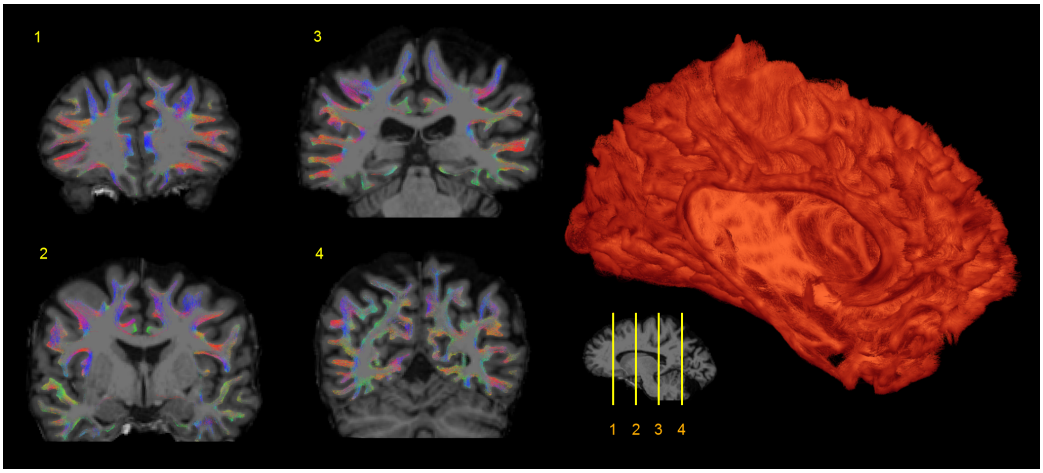

Figure 3: Final appearances of SAF tractograms following the filtering process. **Left:** SAF streamlines overlaid on the T1-weighted volume in dMRI space (coronal view). **Right:** 3D visualisation of SAF streamlines in one hemisphere (medial view). The sagittal slice at the bottom shows positions of the cuts on the left.

overall mean length and FA, respectively. The range of values on the surface in a single subject can be seen in **??**. The overall proportion of streamlines terminating in gyri was 59.21±1.30%, supporting the presence of gyral bias.

Seeding and Filtering Descriptors	**Mean**[1]	**SD**[1]	**CV_W(%)**	**CV_B(%)**	**ICC**
Number of streamlines generated	4.5M	39.1K	1.11	5.50	0.877
Total number of streamlines retained after filtering	0.9M	20.7K	3.56	9.37	0.654
Filtered Tractogram Descriptors[2]					
Streamline length (mm)	19.11	0.14	0.99	0.80	0.000
Mean streamline FA	0.31	0.00	1.28	5.55	0.845
Surface Data Before Filtering[3]					
Cortical coverage (%)	88.43	0.70	1.11	5.42	0.874
Termination density (streamlines/vertex)	18.38	0.27	2.07	3.10	0.985
Surface Data After Filtering[4]					
Cortical coverage (%)	87.26	0.87	1.38	4.27	0.729
Termination density (streamlines/vertex)	6.93	0.15	3.08	3.76	0.978
Mean streamline length per vertex (mm)	17.05	0.25	1.91	6.20	0.749
Mean streamline FA per vertex	0.28	0.01	2.44	9.03	0.796
Prevalence of gyri in the covered surface (%)	59.21	1.30	0.51	2.84	0.904

[1] Averaged within subjects

[2] Averaged over all SAF streamlines of both hemispheres

[3] Calculated at MCC, averaged over all vertices of both hemispheres

[4] Calculated at WSM, averaged over all vertices of both hemispheres

Table 3: Whole-brain metrics. Surface metrics were calculated before smoothing. Measures of consistency were calculated using mean values per session. SD, standard deviation. CV_W, coefficient of variation within subjects. CV_B, coefficient of variation between subjects. ICC, intraclass correlation coefficient. FA, fractional anisotropy.

With the exception of streamline length, all metric means exhibited high reproducibility (CV_W 0.51-3.56%), low between-subject variation (CV_B 0.80-9.37%), and moderate-to-high reliability (ICC 0.654-0.978). Streamline length had a very low standard deviation across the board resulting in similarly low CV_W and CV_B therefore producing a low ICC.

4.3. Track density imaging maps

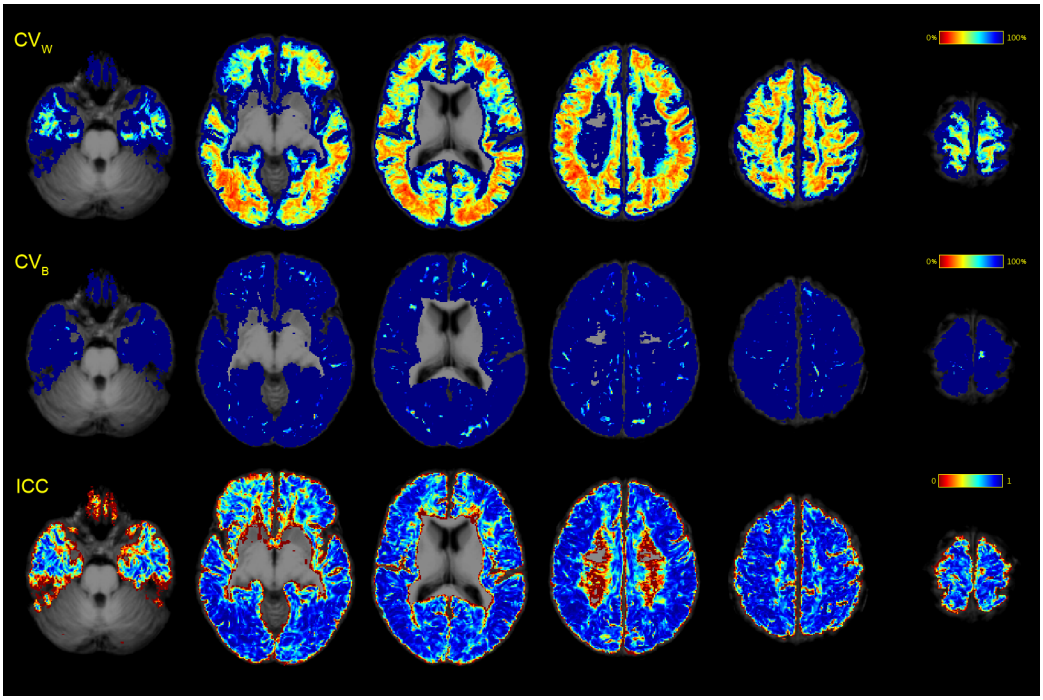

Figure 4: Repeatability of SAF using TDI map comparison in common space. All maps were superimposed on the average T1-weighted volume. Streamlines were truncated at the white matter surface before map generation. CV_W and CV_B were thresholded at 100%. CV_W, coefficient of variation within subjects. CV_B, coefficient of variation between subjects. ICC, intraclass correlation coefficient.

Although TDI maps suggested an overall moderate-to-high reliability of the spatial distribution of streamlines (median ICC: 0.771), reproducibility was low (median CV_W: 66.16%) suggesting a lot of variation within subjects (Figure 4). Median CV_B was 274.76% (thresholded in the figure), attesting to a very high variation between subjects when comparing TDI maps. The immediate subcortical areas showed the least consistency, possibly as a result of cortical folding differences (manifesting in registration imperfections)

coupled with partial volume effects or less reliable tracking on the grey-white interface.

4.4. Surface-based analysis

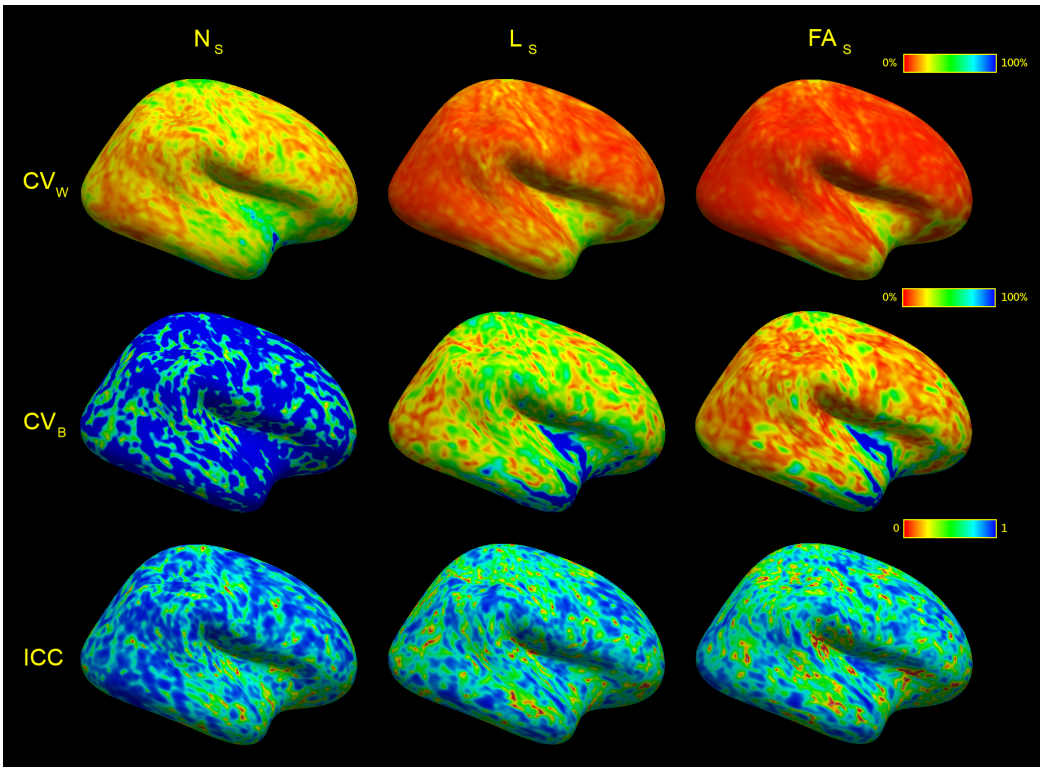

Figure 5: Surface-based analysis demonstrated on the lateral cortex of the right hemisphere. N_S, termination density (number of streamlines/vertex). L_S, mean streamline length/vertex. FA_S, mean streamline fractional anisotropy/vertex. CV_W, coefficient of variation within subjects. CV_B, coefficient of variation between subjects. ICC, intra-class correlation coefficient. Values at each vertex were recorded in subject space, then transformed into average subject space before running analyses. CV_W and CV_B were thresholded at 100%.

In order to minimise the registration-related distortions and issues with

cortical folding differences, streamline data were projected on the surface in native space before applying surface registration (Figure 5, also **??**). Analysis of termination density demonstrated moderate reliability (median ICC: 0.780) and low reproducibility (median CV_W: 27.13%) together with high between-subject variability (median CV_B: 100.35%), although this compared favourably to the results seen with TDI analysis. Similar ICC coefficients and improved coefficients of variation were shown for mean length per vertex (median ICC: 0.666, median CV_W: 12.51%, median CV_B: 38.48%) and mean FA per vertex (median ICC: 0.685, median CV_W: 8.02%, median CV_B: 22.31%). Fronto- and temporo-basal areas showed the least consistency, likely a result of susceptibility distortions arising from the EPI-readout used for the dMRI and T1-dMRI misalignment in those regions. Gyral bias appeared to also contribute to regional differences in consistency, with sulcal areas exhibiting higher reproducibility and reliability (Table 4).

4.5. Graph theory metrics

SAF tractograms were also examined from a network perspective using graph theory properties (Table 5). As SAF are structured to subserve local connectivity, it is likely that the vast majority of edges occurred between the neighbouring nodes only, creating a network that can be viewed as a regular lattice (low cost, low efficiency). As expected, irrespective of the parcellation used these networks resulted in a very low clustering coefficient, global efficiency and averaged local efficiency, with a similar average network strength. Additionally, HCP-MMP1 had more parcels each having fewer immediate neighbours which further reduced lattice dimensionality; as such, lower average network density, decreased average betweenness centrality and a longer

Data on the surface[1]	**CV_W: gyri (%)**	**CV_W: sulci (%)**	**p**[2]
Termination count after filtering:	31.87±19.41	30.97±18.12	0.000
Mean streamline length per vertex:	16.43±15.25	15.95±15.14	0.000
Mean streamline FA per vertex:	11.56±13.14	11.19±13.02	0.000

Data on the surface[1]	**CV_B: gyri (%)**	**CV_B: sulci (%)**	**p**[2]
Termination count after filtering:	106.92±42.87	106.32±44.21	0.000
Mean streamline length per vertex:	47.4±32.99	46.47±34.21	0.000
Mean streamline FA per vertex:	32.3±30.53	31.88±32.17	0.000

Data on the surface[1]	**ICC: gyri**	**ICC: sulci**	**p**[2]
Termination count after filtering:	0.723±0.200	0.728±0.195	0.000
Mean streamline length per vertex:	0.666±0.205	0.666±0.202	0.913
Mean streamline FA per vertex:	0.641±0.209	0.646±0.205	0.000

[1] Definitions as in Table 3

[2] Two-sample T-test (two-tailed)

Table 4: Reproducibility of surface-projected streamline data in relation to cortical morphology and the effects of the gyral bias. Data are presented as mean±SD across all gyral or sulcal vertices. CV_W, coefficient of variation within subjects. CV_B, coefficient of variation between subjects. ICC, intraclass correlation coefficient.

characteristic path length were observed with this parcellation. For either of the two schemes, network properties were similar across hemispheres.

From the tractogram consistency perspective, it is worth noting that due to DKT's larger parcel areas more streamlines were discarded as they occurred within, not between, parcels. In general, DKT demonstrated moderate reproducibility (CV_W: 3.49-13.02%) and variable reliability (ICC: 0.000-0.838) depending on the metric used. On the other hand, HCP-MMP1 showed slightly lower reproducibility (CV_W: 2.54-20.09%) but higher reliability (ICC: 0.496-0.945). Further, on the whole the metrics appeared more consistent in the left hemisphere compared to the right when DKT was used

while with HCP-MMP1 the right hemisphere exhibited greater reproducibility but lower reliability.

DKT	**Right hemisphere**					**Left hemisphere**				
	Mean[1]	**SD**[1]	**CV_W(%)**	**CV_B(%)**	**ICC**	**Mean**[1]	**SD**[1]	**CV_W(%)**	**CV_B(%)**	**ICC**
Network density[2]	0.30	0.01	3.49	13.39	0.809	0.31	0.01	3.98	16.81	0.838
Network strength[2]	0.24	0.02	9.66	17.03	0.424	0.28	0.02	7.55	24.68	0.751
Betweenness centrality[2]	0.11	0.00	4.64	14.26	0.725	0.10	0.00	4.78	13.76	0.696
Clustering coefficient	0.01	0.00	13.02	10.54	0.000	0.01	0.00	11.98	29.74	0.623
Characteristic path length	69.70	6.54	12.25	22.23	0.442	56.88	3.55	7.93	13.42	0.398
Global efficiency	0.02	0.00	9.02	16.18	0.435	0.03	0.00	7.61	29.08	0.807
Local efficiency[2]	0.01	0.00	12.67	10.26	0.000	0.01	0.00	11.73	30.67	0.650

HCP-MMP1	**Right hemisphere**					**Left hemisphere**				
	Mean[1]	**SD**[1]	**CV_W(%)**	**CV_B(%)**	**ICC**	**Mean**[1]	**SD**[1]	**CV_W(%)**	**CV_B(%)**	**ICC**
Network density[2]	0.11	0.00	2.54	19.26	0.945	0.11	0.00	3.12	20.76	0.929
Network strength[2]	0.25	0.03	13.87	27.55	0.496	0.27	0.04	18.87	47.85	0.634
Betweenness centrality[2]	0.04	0.00	4.49	18.10	0.824	0.04	0.00	4.96	17.55	0.781
Clustering coefficient	0.00	0.00	15.56	49.35	0.738	0.00	0.00	19.19	80.04	0.834
Characteristic path length	184.71	24.41	17.66	36.61	0.522	175.06	26.59	20.09	42.82	0.538
Global efficiency	0.01	0.00	14.61	31.75	0.550	0.01	0.00	20.05	56.79	0.689
Local efficiency[2]	0.01	0.00	15.70	50.07	0.740	0.01	0.00	19.34	80.79	0.834

[1] Averaged within subjects

[2] Averaged across all nodes

Table 5: Graph theory metrics using two different parcellation schemes. By definition, hemispheres shared no connections and were examined separately. DKT, Desikan-Killiany parcellation. HCP-MMP1, Human Connectome Project multi-modal parcellation. SD, standard deviation. CV_W, coefficient of variation within subjects. CV_B, coefficient of variation between subjects. ICC, intraclass correlation coefficient.

5. Discussion

5.1. Novelty of the work

The work presented herein offers a novel approach to short association fibre analysis by marrying tractography with mesh representation of the cortex motivated by the close association of SAF with the latter. We were specifically interested in studying the shorter pathways (consistent with the definition in Schüz and Braitenberg (2002) as these pathways are particularly sensitive to inter-individual cortical folding variations (Bajada et al. (2019)) and harder to study using the more established approaches (Román et al. (2017); Zhang et al. (2018); Guevara et al. (2017); Van Essen et al. (2014)). We believe that this study adds a number of useful contributions to the literature.

First, the framework introduces simple yet strong anatomical constraints which operate in an unbiased fashion on a whole-brain level and require no filters that could lead to exclusion of otherwise valid structures (e.g., not dependent on streamline shape or cortical parcellation). The resulting tractograms show streamline distribution and trajectories in keeping with an anatomical definition (Schüz and Braitenberg (2002)) of SAF without the need for manual pruning of noisy streamlines. The framework is modular and easily adaptable, enabling its use for studying SAF across a range of physiological and pathological conditions. It supports the use of a surface-based seeding approach as employed here but will also filter tractograms that were obtained with other means if desired. Using a bespoke algorithm, termination points of each streamline on the cortical mesh are registered during filtering, allowing direct interfacing between any streamline- and surface-

related metrics (without reliance on the voxel grid) for subsequent analyses.

Second, we present a thorough evaluation of the tractograms generated with this method using state-of-the-art repeatability data (Koller et al. (2020)). The description process is broadly divided into streamline-, voxel-, surface- and network-wise assessments, to our knowledge representing the most complete characterisation of whole-brain SAF tractograms to date. This includes measures of fractional anisotropy chosen as exemplar scalar to showcase performance of the pipeline for microstructure analysis; in future studies, a more exhaustive profiling of SAF microstructure may be conducted. The use of volume- and surface-based approaches allows to examine the differences in SAF properties on a regional level. We also conceptualised SAF as a network and provided graph theory analysis comparing two different parcellation schemes, which to our knowledge has not been done before. While we did not utilise semi-global streamline optimisation algorithms (Smith et al. (2015); Daducci et al. (2015)) nor normalise edge weights by parcel areas, this still forms a useful baseline and informs future work.

Third, our approach to the representation of SAF metrics on the surface merits its own mention. Projection of streamline-related data on surface vertices is not new (Li et al. (2010); Chen et al. (2012); Bajada et al. (2019); Padula et al. (2017)); however, usually this has been achieved by searching for all streamlines within a (typically) large sphere around a WSM vertex which risks decreased specificity and leads to overlaps. In regions where non-continuous parts of the cortical mantle lie in close proximity with each other (such as the opposite banks of a narrow gyrus), erroneous inclusion of streamlines that terminate near remote vertices may occur. Alternatively,

streamline density (Li et al. (2010); Nie et al. (2011)) and orientation termination (Chen et al. (2012)) around a surface vertex have been quantified as the number/orientation of streamlines penetrating the adjacent faces normalised by the combined surface area of the faces. While representing a more robust way to record these data on the surface, the latter approach allows for overlapping between adjacent vertices and, more importantly, on its own does not account for the streamlines not reaching the cortical mesh resulting in strong gyral bias. On the other hand, our method represents a significant improvement through the following combination: (1) allowing some propagation of streamlines into the cortex during seeding (later truncated at the interface) ensures more intersections of streamlines with the surface occur; (2) limiting the inclusion sphere to the local cortical thickness during filtering increases specificity of streamline-surface mapping; (3) subsequent fine-scale searching for intersections at the grey-white interface results in unique allocation of vertices based on proximity such that each streamline end is only associated with one vertex. This combination may lead to rejection of streamlines approaching but not entering the cortex (Yeh et al. (2019)); however, the proportion of such streamlines appeared negligible based on the distribution of rejected termination points (**??**) with an overall weak gyral bias (Table 3 and Table 4). Further, increased sensitivity could be achieved by expanding the WSM inwards during filtering using e.g. mean-curvature flow (St-Onge et al. (2018)), although this may lead to false positives in certain regions as, for example, the predominant orientation of axonal fibres around sulcal fundi is near-tangential and thus the "passing" fibres may be erroneously included; hence this extra step was not pursued. Depending on the

analyses of interest, subsequent smoothing on the surface may be applied as performed in this study. Further, projection of certain types of data (such as mean scalar measures along a streamline, e.g. fractional anisotropy) may not be justified in the context of whole-brain or deep-bundle tractography where many streamlines run at a distance from the cortex and exhibit vastly varying trajectories; on the other hand, this "collapsing" of data seems natural with SAF due to their short length and course that is inevitably local to the vertex to which data are being projected. Comparison of data represented in this way is achieved through surface registration which can handle cortical folding differences better than volume registration (critical when dealing with the immediate subcortical structures) with all other steps performed in native dMRI space. Finally, surface-based analysis provides the option of using per-vertex or cluster-based statistical comparison methods, circumventing the use of cortical parcellation if desired and therefore avoiding the associated issues of lower sensitivity within and artificial boundaries between cortical regions.

5.2. Consistency of SAF tractograms

Our analysis is complemented by a detailed evaluation of whole-brain SAF for consistency, including evaluation of reproducibility, reliability and between-subject variability. This demonstrated varying results depending on the approach taken. High overall reproducibility and reliability of streamline counts in the initial (not SAF-specific) tractograms dropped slightly as a result of filtering while still remaining within a good range. Streamline count is influenced by a multitude of factors, most of which can play a role at both the initial tractogram generation and filtering. Hence, on its own

this may not be a good indicator of tractogram consistency. Instead, the number vertices with streamlines (cortical coverage) or number of streamlines per vertex (termination density) are possibly more insightful; in this work, reproducibility and reliability of both was high. On the other hand, mean streamline length demonstrated very low reliability. Here, the overall variance was so low that any within- and between-subject differences were likely at the noise level, suggesting that the whole-brain averaged length was not a useful measure for comparison. Indeed, examining streamline length at the vertex level yielded more informative results. As expected (Zhang et al. (2010)), track density imaging maps demonstrated large variability in the spatial distribution of SAF between individuals but also within individuals; in the attempt to minimise the role of registration imperfections and partial volume effects, alternative measures such as regional density and mean streamline length of SAF were compared by projecting them on the surface resulting in improved consistency. Our approach does not perform a dedicated removal of noisy (false positive) streamlines relying only on the anatomical constraints, and it is therefore probable that a proportion of variability within and between subjects is explained by the occurrence of such streamlines owing to the fundamental limitations of a chosen tractography algorithm. The lack of detailed histological or tracer injection validation data for SAF on the whole-brain scale makes identification and exclusion of such streamlines difficult; development of better scanning hardware and tractography/optimisation algorithms will facilitate greater fidelity of the tractograms.

Consistency of whole-brain SAF representation with dMRI-based stream-

lines tractography approaches has previously been addressed. Zhang et al. (2010) used diffusion tensor imaging (DTI)-based deterministic tractography to create an atlas and a probabilistic spatial map of multiple white matter tracts, including all short association fibres connecting 24 regions obtained from a superficial white matter parcellation. Having detected 29 connections present in all 20 individuals studied, they emphasised large spatial variability (demonstrated but not quantified) and the difficulty in manual region-of-interest segmentation of these tracts advocating for an automated approach. In another study (Zhang et al. (2014)), shape-driven filtering and a further criterion of proximity to sulcal fundi were used to examine U-fibres across diffusion spectrum imaging (DSI), high angular resolution diffusion imaging (HARDI) and DTI data sets with deterministic streamlines tracking. Based on normalised streamline counts, the authors demonstrated an overall stronger short-range than middle-range connectivity with HARDI and DSI data and the reverse with DTI data, proposing the inability of the latter to detect crossing fibres and therefore more false negatives as the likely mechanism. Guevara et al. (2017) used DKT-based parcellation and shape- and distance-based clustering of larger streamlines (centroids 20-80 mm) in Talairach space to identify 100 distinct bundles (50 per hemisphere, 35 common to both) that were considered to have low-to-moderate variability (relative standard deviation (RSD) ≤ 0.9) in streamline counts and shape across two test and one validation data sets. This method was further improved by using non-linear registration and ability to detect within-region connections (Román et al. (2017)); clustering larger (centroids 35-85 mm) streamlines and using a bagging strategy, the authors successfully constructed an

atlas of 93 SAF bundles (44 in left hemisphere, 49 in right, 33 common) with repeatability of individual bundles ranging between 8/10 and 10/10. Zhang et al. (2018) generated an atlas of white matter pathways based on 100 Human Connectome Project (HCP) subjects using two-tensor unscented Kalman filter for tracking and groupwise tractography registration followed by groupwise spectral clustering. Their approach did not require the use of a cortical parcellation. A total of 58 deep and 198 short and medium range superficial clusters were identified, although no further detailed description of the latter was provided. The classification was subsequently applied to a number of additional data sets with variable acquisition methods, spanning different age ranges and including clinical cohorts. Depending on the data set examined, this approach identified 92.28-99.96% of the "superficial" clusters on the subject level, with the average between-subject CV of 0.488-0.919 for streamline counts/cluster, and the average overlap between subject and atlas clusters of 0.747-0.783 (as determined using intersected FreeSurfer regions). Subsequent work (Guevara et al. (2020)) compared the three atlases (Guevara et al. (2017); Román et al. (2017); Zhang et al. (2018)) in MNI space for bundle similarity by computing the maximum Euclidean distance between corresponding points for each streamline in a bundle to all the streamlines in another bundle. With cut-offs for distance and percentage of similar streamlines of 8 mm and $\leq$ 80%, respectively, there was a good overlap between the bundles, particularly in frontal and parietal areas, the atlas of Zhang et al. (2018) contained 96 bundles not present in the other two atlases. The same paper compared the impact of different tractography algorithms (DTI, generalized Q-sampling imaging or GQI and MRtrix iFOD2

using ACT+SIFT) on consistency of clustering, showing that the probabilistic tracking with MRtrix was able to reconstruct all bundles in 100% of cases with a greater spatial coverage but with a higher streamline count RSD compared to the other algorithms. As mentioned previously, these streamline clustering approaches appear to show a good performance when classifying the larger cortical connections but are not typically applied to the smaller ones. While not studying SAF on a whole-brain scale, the study by Movahedian Attar et al. (2020) is of special interest as similarly to our work it relied on the length definition of Schüz and Braitenberg (2002) and used dMRI data acquired using ultra-high gradient Connectom scanner (choosing higher spatial resolution over higher b-values). The study evaluated connectivity (using relative streamline counts) within the occipital cortex as defined by fMRI regions-of-interest and demonstrated a test-retest ICC of 0.73±0.33 (0.88±0.70 for "retinotopic" and 0.69±0.35 for "non-retinotopic", considered false positive by design, bundles) and an averaged CoV of 0.23 (0.23±0.23 for "retinotopic" and 0.25±0.14 for "non-retinotopic" bundles). The use of multimodal surface registration algorithms allowing integration of structural and functional units of the cortex (Robinson et al. (2014)) resulting in similar assessments on a whole-brain scale is a future interest to extend our work.

5.3. Limitations

Some limitations of the proposed approach should be mentioned. First, the dMRI repeatability data used in this study had a voxel size of 2x2x2 mm^3. While previous work has suggested the ideal voxel size below 0.9 mm (isotropic) to remain sensitive to the smaller component of SAF (Song et al. (2014); Movahedian Attar et al. (2020)), the voxel size used in our cohort is

representative of what is commonly used in diffusion studies; further, our data were acquired with higher b-values and using high angular resolution, increasing sensitivity to the intra-axonal component of the white matter (Novikov et al. (2019); Vos et al. (2016)) while maintaining a good signal-to-noise ratio due to the use of high gradient strength (Jones et al. (2018)). We also upsampled our data as it has been shown to improve the geometrical representation of white matter tracts (Dyrby et al. (2014); Shastin et al. (2019)). The second limitation is the sensitivity of the framework to registration quality between T1-weighted and dMRI data. Data sets containing distortions (such as susceptibility artifact) or unusual anatomy (e.g., tumours) are likely to have a mismatch between the surfaces reconstructed from T1-weighted images and the white matter signal on dMRI. As such, visual inspection is crucial on an individual basis although we did not encounter any issues with registration. dMRI-based surface extraction could offer an alternative solution (Liu et al. (2007); Li et al. (2010); Shastin et al. (2020)) if performed at sufficiently high resolution. Third, the current approach to surface seeding precludes the use of semi-global streamline optimisation algorithms (Smith et al. (2015); Daducci et al. (2015)) which require whole-brain tractograms. This limitation can be easily overcome by including the remaining grey matter structures (subcortical grey, cerebellar cortex, amygdalae, and hippocampi) into the array of seeding coordinates and applying the optimisation algorithms before subsequent filtering, preserving streamline weights throughout the process. Finally, as mentioned previously, this paper used the length definition of SAF as under 40 mm minus the variable intracortical section (mean 19.11$\pm$0.14 mm). While application of our method without

this additional criterion resulted in a similar (albeit denser) tractogram appearances and was dominated by short streamlines (mean ≈30 mm, data not shown, consistent with Padula et al. (2017)), it could be similarly used to study larger subcortical association fibres although extra filters such as passage in the vicinity of sulci (Zhang et al. (2014)) may be needed.

6. Conclusions

Our novel superficial association fibres tractography framework consistently showed large cortical coverage facilitating surface-based comparisons. We characterised SAF and assessed their consistency using a variety of complimentary approaches, supporting the framework as the plausible vehicle for investigating SAF in health as well as in clinical cohorts.

Declarations of interest: none

Author contributions

Dmitri Shastin: conceptualization, methodology, software, validation, formal analysis, writing - original draft, writing - review & editing, visualization, funding acquisition. Sila Genc: methodology, software, writing - original draft. Greg D. Parker: conceptualization, software. Kristin Koller: resources, data curation. Chantal M.W. Tax: methodology, writing - review & editing. John Evans: resources, methodology. Khalid Hamandi: writing - review & editing, supervision. William P. Gray: writing - review & editing, conceptualization, supervision. Derek K. Jones: conceptualization, writing

- original draft, writing - review & editing, supervision. Maxime Chamberland: conceptualization, writing - original draft, writing - review & editing, visualization, supervision.

Acknowledgements

This research was funded by the Wellcome Trust [220537/Z/20/Z, 096646/Z/11/Z, 104943/Z/14/Z, 215944/Z/19/Z], the Engineering and Physical Sciences Research Council [EP/M029778/1], the Dutch Research Council [17331], a Radboud Excellence Initiative Fellowship, and the Brain Repair and Intracranial Neurotherapeutics (BRAIN) Unit funded by Health and Care Research Wales. For the purpose of open access, the author has applied a CC BY public copyright licence to any Author Accepted Manuscript version arising from this submission.

DS would like to thank Prof. Peter H. Morgan at Cardiff Business School for discussions about statistics.

References

Andersson, J.L., Skare, S., Ashburner, J., 2003. How to correct susceptibility distortions in spin-echo echo-planar images: application to diffusion tensor imaging. Neuroimage 20, 870–88. doi:10.1016/S1053-8119(03)00336-7.

Andersson, J.L.R., Sotiropoulos, S.N., 2016. An integrated approach to correction for off-resonance effects and subject movement in diffusion mr imaging. Neuroimage 125, 1063–1078. doi:10.1016/j.neuroimage.2015.10.019.

Arthur, D., Vassilvitskii, S., 2006. k-means++: The Advantages of Careful Seeding. techreport. Stanford InfoLab.

Assaf, Y., Johansen-Berg, H., Thiebaut de Schotten, M., 2019. The role of diffusion mri in neuroscience. NMR in Biomedicine 32, e3762.

Avants, B.B., Tustison, N., Song, G., 2009. Advanced normalization tools (ants). Insight j 2, 1–35.

Bajada, C.J., Schreiber, J., Caspers, S., 2019. Fiber length profiling: A novel approach to structural brain organization. Neuroimage 186, 164–173.

Calamante, F., Tournier, J.D., Jackson, G.D., Connelly, A., 2010. Track-density imaging (tdi): super-resolution white matter imaging using whole-brain track-density mapping. Neuroimage 53, 1233–1243.

Chen, G., Taylor, P.A., Haller, S.P., Kircanski, K., Stoddard, J., Pine, D.S., Leibenluft, E., Brotman, M.A., Cox, R.W., 2018. Intraclass correlation:

Improved modeling approaches and applications for neuroimaging. Human brain mapping 39, 1187–1206.

Chen, H., Zhang, T., Guo, L., Li, K., Yu, X., Li, L., Hu, X., Han, J., Hu, X., Liu, T., 2012. Coevolution of Gyral Folding and Structural Connection Patterns in Primate Brains. Cerebral Cortex 23, 1208–1217. doi:10.1093/cercor/bhs113.

Daducci, A., Dal Palu, A., Lemkaddem, A., Thiran, J.P., 2015. Commit: Convex optimization modeling for microstructure informed tractography. IEEE Trans Med Imaging 34, 246–57. doi:10.1109/TMI.2014.2352414.

Datta, G., Colasanti, A., Rabiner, E.A., Gunn, R.N., Malik, O., Ciccarelli, O., Nicholas, R., Van Vlierberghe, E., Van Hecke, W., Searle, G., et al., 2017. Neuroinflammation and its relationship to changes in brain volume and white matter lesions in multiple sclerosis. Brain 140, 2927–2938.

Dell'Acqua, F., Tournier, J., 2017. Reconstructing fiber orientations with diffusion mri. NMR Biomed .

Dhollander, T., Raffelt, D., Connelly, A., 2016. Unsupervised 3-tissue response function estimation from single-shell or multi-shell diffusion mr data without a co-registered t1 image, in: ISMRM Workshop on Breaking the Barriers of Diffusion MRI, p. 5.

Dubois, J., Dehaene-Lambertz, G., Kulikova, S., Poupon, C., Hüppi, P.S., Hertz-Pannier, L., 2014. The early development of brain white matter: a review of imaging studies in fetuses, newborns and infants. Neuroscience 276, 48–71.

Dyrby, T.B., Lundell, H., Burke, M.W., Reislev, N.L., Paulson, O.B., Ptito, M., Siebner, H.R., 2014. Interpolation of diffusion weighted imaging datasets. Neuroimage 103, 202–213. doi:10.1016/j.neuroimage.2014.09.005.

d'Albis, M.A., Guevara, P., Guevara, M., Laidi, C., Boisgontier, J., Sarrazin, S., Duclap, D., Delorme, R., Bolognani, F., Czech, C., et al., 2018. Local structural connectivity is associated with social cognition in autism spectrum disorder. Brain 141, 3472–3481.

Fischl, B., 2012. Freesurfer. Neuroimage 62, 774–781.

Fischl, B., Sereno, M.I., Tootell, R.B., Dale, A.M., 1999. High-resolution intersubject averaging and a coordinate system for the cortical surface. Hum Brain Mapp 8, 272–84. doi:10.1002/(sici)1097-0193(1999)8:4<272::aid-hbm10>3.0.co;2-4.

Genc, S., Tax, C.M., Raven, E.P., Chamberland, M., Parker, G.D., Jones, D.K., 2020. Impact of b-value on estimates of apparent fibre density. Human brain mapping 41, 2583–2595.

Glasser, M.F., Coalson, T.S., Robinson, E.C., Hacker, C.D., Harwell, J., Yacoub, E., Ugurbil, K., Andersson, J., Beckmann, C.F., Jenkinson, M., et al., 2016. A multi-modal parcellation of human cerebral cortex. Nature 536, 171–178.

Glasser, M.F., Sotiropoulos, S.N., Wilson, J.A., Coalson, T.S., Fischl, B., Andersson, J.L., Xu, J., Jbabdi, S., Webster, M., Polimeni, J.R., Van Essen, D.C., Jenkinson, M., Consortium, W.U.M.H., 2013. The minimal

preprocessing pipelines for the human connectome project. Neuroimage 80, 105–24. doi:10.1016/j.neuroimage.2013.04.127.

Govindan, R.M., Asano, E., Juhasz, C., Jeong, J.W., Chugani, H.T., 2013. Surface-based laminar analysis of diffusion abnormalities in cortical and white matter layers in neocortical epilepsy. Epilepsia 54, 667–77. doi:10.1111/epi.12129.

de Groot, M., Ikram, M.A., Akoudad, S., Krestin, G.P., Hofman, A., van der Lugt, A., Niessen, W.J., Vernooij, M.W., 2015. Tract-specific white matter degeneration in aging: the rotterdam study. Alzheimer's & Dementia 11, 321–330.

Guevara, M., Guevara, P., Roman, C., Mangin, J.F., 2020. Superficial white matter: A review on the dmri analysis methods and applications. Neuroimage 212, 116673. doi:10.1016/j.neuroimage.2020.116673.

Guevara, M., Roman, C., Houenou, J., Duclap, D., Poupon, C., Mangin, J.F., Guevara, P., 2017. Reproducibility of superficial white matter tracts using diffusion-weighted imaging tractography. Neuroimage 147, 703–725. doi:10.1016/j.neuroimage.2016.11.066.

Hihara, S., Notoya, T., Tanaka, M., Ichinose, S., Ojima, H., Obayashi, S., Fujii, N., Iriki, A., 2006. Extension of corticocortical afferents into the anterior bank of the intraparietal sulcus by tool-use training in adult monkeys. Neuropsychologia 44, 2636–2646.

Jeurissen, B., Descoteaux, M., Mori, S., Leemans, A., 2017. Diffusion mri fiber tractography of the brain. NMR Biomed doi:10.1002/nbm.3785.

Jeurissen, B., Tournier, J.D., Dhollander, T., Connelly, A., Sijbers, J., 2014. Multi-tissue constrained spherical deconvolution for improved analysis of multi-shell diffusion mri data. Neuroimage 103, 411–426. doi:10.1016/j.neuroimage.2014.07.061.

Jones, D.K., Alexander, D.C., Bowtell, R., Cercignani, M., Dell'Acqua, F., McHugh, D.J., Miller, K.L., Palombo, M., Parker, G.J.M., Rudrapatna, U.S., Tax, C.M.W., 2018. Microstructural imaging of the human brain with a 'super-scanner': 10 key advantages of ultra-strong gradients for diffusion mri. Neuroimage 182, 8–38. doi:10.1016/j.neuroimage.2018.05.047.

Kai, J., Khan, A.R., 2019. Assessing white matter pathway reproducibility from human whole-brain tractography clustering. bioRxiv .

Kellner, E., Dhital, B., Kiselev, V.G., Reisert, M., 2016. Gibbs-ringing artifact removal based on local subvoxel-shifts. Magn Reson Med 76, 1574–1581. doi:10.1002/mrm.26054.

Koller, K., Rudrapatna, S.U., Chamberland, M., Raven, E.P., Parker, G.D., Tax, C.M., Drakesmith, M., Fasan, F., Owen, D., Hughes, G., et al., 2020. Micra: Microstructural image compilation with repeated acquisitions. NeuroImage , 117406.

Laguna, P.A.L., Combes, A.J., Streffer, J., Einstein, S., Timmers, M., Williams, S.C., Dell'Acqua, F., 2020. Reproducibility, reliability and variability of fa and md in the older healthy population: A test-retest multiparametric analysis. NeuroImage: Clinical 26.

Li, K., Guo, L., Li, G., Nie, J., Faraco, C., Cui, G., Zhao, Q., Miller, L.S., Liu, T., 2010. Gyral folding pattern analysis via surface profiling. NeuroImage 52, 1202–1214.

Liu, M., Bernhardt, B.C., Hong, S.J., Caldairou, B., Bernasconi, A., Bernasconi, N., 2016. The superficial white matter in temporal lobe epilepsy: a key link between structural and functional network disruptions. Brain 139, 2431–40. doi:10.1093/brain/aww167.

Liu, T., Li, H., Wong, K., Tarokh, A., Guo, L., Wong, S.T., 2007. Brain tissue segmentation based on dti data. NeuroImage 38, 114 – 123. doi:https://doi.org/10.1016/j.neuroimage.2007.07.002.

Maier-Hein, K.H., Neher, P.F., Houde, J.C., Cote, M.A., Garyfallidis, E., Zhong, J., Chamberland, M., Yeh, F.C., Lin, Y.C., Ji, Q., Reddick, W.E., Glass, J.O., Chen, D.Q., Feng, Y., Gao, C., Wu, Y., Ma, J., He, R., Li, Q., Westin, C.F., Deslauriers-Gauthier, S., Gonzalez, J.O.O., Paquette, M., St-Jean, S., Girard, G., Rheault, F., Sidhu, J., Tax, C.M.W., Guo, F., Mesri, H.Y., David, S., Froeling, M., Heemskerk, A.M., Leemans, A., Bore, A., Pinsard, B., Bedetti, C., Desrosiers, M., Brambati, S., Doyon, J., Sarica, A., Vasta, R., Cerasa, A., Quattrone, A., Yeatman, J., Khan, A.R., Hodges, W., Alexander, S., Romascano, D., Barakovic, M., Auria, A., Esteban, O., Lemkaddem, A., Thiran, J.P., Cetingul, H.E., Odry, B.L., Mailhe, B., Nadar, M.S., Pizzagalli, F., Prasad, G., Villalon-Reina, J.E., Galvis, J., Thompson, P.M., Requejo, F.S., Laguna, P.L., Lacerda, L.M., Barrett, R., Dell'Acqua, F., Catani, M., Petit, L., Caruyer, E., Daducci, A., Dyrby, T.B., Holland-Letz, T., Hilgetag, C.C.,

Stieltjes, B., Descoteaux, M., 2017. The challenge of mapping the human connectome based on diffusion tractography. Nat Commun 8, 1349. doi:10.1038/s41467-017-01285-x.

Markov, N.T., Ercsey-Ravasz, M., Ribeiro Gomes, A., Lamy, C., Magrou, L., Vezoli, J., Misery, P., Falchier, A., Quilodran, R., Gariel, M., et al., 2014. A weighted and directed interareal connectivity matrix for macaque cerebral cortex. Cerebral cortex 24, 17–36.

McGraw, K.O., Wong, S.P., 1996. Forming inferences about some intraclass correlation coefficients. Psychological methods 1, 30.

Mills, K., 2016. Hcp-mmp1.0 projected on fsaverage. doi:10.6084/m9.figshare.3498446.v2.

Mito, R., Raffelt, D., Dhollander, T., Vaughan, D.N., Tournier, J.D., Salvado, O., Brodtmann, A., Rowe, C.C., Villemagne, V.L., Connelly, A., 2018. Fibre-specific white matter reductions in alzheimer's disease and mild cognitive impairment. Brain 141, 888–902.

Mori, S., Van Zijl, P.C., 2002. Fiber tracking: principles and strategies–a technical review. NMR in Biomedicine: An International Journal Devoted to the Development and Application of Magnetic Resonance In Vivo 15, 468–480.

Movahedian Attar, F., Kirilina, E., Haenelt, D., Pine, K.J., Trampel, R., Edwards, L.J., Weiskopf, N., 2020. Mapping short association fibers in the early cortical visual processing stream using in vivo diffusion tractography. Cereb Cortex doi:10.1093/cercor/bhaa049.

Nazeri, A., Chakravarty, M.M., Felsky, D., Lobaugh, N.J., Rajji, T.K., Mulsant, B.H., Voineskos, A.N., 2013. Alterations of superficial white matter in schizophrenia and relationship to cognitive performance. Neuropsychopharmacology 38, 1954–1962.

Neubert, F.X., Mars, R.B., Buch, E.R., Olivier, E., Rushworth, M.F.S., 2010. Cortical and subcortical interactions during action reprogramming and their related white matter pathways. Proceedings of the National Academy of Sciences 107, 13240–13245. doi:10.1073/pnas.1000674107.

Nie, J., Guo, L., Li, K., Wang, Y., Chen, G., Li, L., Chen, H., Deng, F., Jiang, X., Zhang, T., Huang, L., Faraco, C., Zhang, D., Guo, C., Yap, P.T., Hu, X., Li, G., Lv, J., Yuan, Y., Zhu, D., Han, J., Sabatinelli, D., Zhao, Q., Miller, L.S., Xu, B., Shen, P., Platt, S., Shen, D., Hu, X., Liu, T., 2011. Axonal Fiber Terminations Concentrate on Gyri. Cerebral Cortex 22, 2831–2839. doi:10.1093/cercor/bhr361.

Novikov, D.S., Fieremans, E., Jespersen, S.N., Kiselev, V.G., 2019. Quantifying brain microstructure with diffusion mri: Theory and parameter estimation. NMR in Biomedicine 32, e3998.

O'Halloran, R., Feldman, R., Marcuse, L., Fields, M., Delman, B., Frangou, S., Balchandani, P., 2017. A method for u-fiber quantification from 7 t diffusion-weighted mri data tested in patients with nonlesional focal epilepsy. Neuroreport 28, 457–461. doi:10.1097/WNR.0000000000000788.

Ouyang, M., Kang, H., Detre, J.A., Roberts, T.P., Huang, H., 2017. Short-range connections in the developmental connectome during typical and

atypical brain maturation. Neuroscience & Biobehavioral Reviews 83, 109–122.

Padula, M.C., Schaer, M., Scariati, E., Mutlu, A.K., Zöller, D., Schneider, M., Eliez, S., 2017. Quantifying indices of short-and long-range white matter connectivity at each cortical vertex. PloS one 12, e0187493.

Phillips, O.R., Clark, K.A., Luders, E., Azhir, R., Joshi, S.H., Woods, R.P., Mazziotta, J.C., Toga, A.W., Narr, K.L., 2013. Superficial white matter: effects of age, sex, and hemisphere. Brain Connect 3, 146–59. doi:10.1089/brain.2012.0111.

Phillips, O.R., Joshi, S.H., Narr, K.L., Shattuck, D.W., Singh, M., Di Paola, M., Ploner, C.J., Pruss, H., Paul, F., Finke, C., 2018. Superficial white matter damage in anti-nmda receptor encephalitis. J Neurol Neurosurg Psychiatry 89, 518–525. doi:10.1136/jnnp-2017-316822.

Phillips, O.R., Nuechterlein, K.H., Asarnow, R.F., Clark, K.A., Cabeen, R., Yang, Y., Woods, R.P., Toga, A.W., Narr, K.L., 2011. Mapping cortico-cortical structural integrity in schizophrenia and effects of genetic liability. Biol Psychiatry 70, 680–9. doi:10.1016/j.biopsych.2011.03.039.

Rademacher, J., 2002. Topographical variability of cytoarchitectonic areas, in: Cortical Areas. CRC Press, pp. 65–90.

Reuter, M., Schmansky, N.J., Rosas, H.D., Fischl, B., 2012. Within-subject template estimation for unbiased longitudinal image analysis. Neuroimage 61, 1402–1418.

Reveley, C., Seth, A.K., Pierpaoli, C., Silva, A.C., Yu, D., Saunders, R.C., Leopold, D.A., Ye, F.Q., 2015. Superficial white matter fiber systems impede detection of long-range cortical connections in diffusion mr tractography. Proc Natl Acad Sci U S A 112, E2820–8. doi:10.1073/pnas.1418198112.

Rheault, F., Poulin, P., Valcourt Caron, A., St-Onge, E., Descoteaux, M., 2020. Common misconceptions, hidden biases and modern challenges of dmri tractography. J Neural Eng doi:10.1088/1741-2552/ab6aad.

Robinson, E.C., Jbabdi, S., Glasser, M.F., Andersson, J., Burgess, G.C., Harms, M.P., Smith, S.M., Van Essen, D.C., Jenkinson, M., 2014. Msm: a new flexible framework for multimodal surface matching. Neuroimage 100, 414–426.

Román, C., Guevara, M., Valenzuela, R., Figueroa, M., Houenou, J., Duclap, D., Poupon, C., Mangin, J.F., Guevara, P., 2017. Clustering of whole-brain white matter short association bundles using hardi data. Frontiers in neuroinformatics 11, 73.

Rubinov, M., Sporns, O., 2010. Complex network measures of brain connectivity: uses and interpretations. Neuroimage 52, 1059–1069.

Sairanen, V., Leemans, A., Tax, C.M.W., 2018. Fast and accurate slicewise outlier detection (solid) with informed model estimation for diffusion mri data. Neuroimage 181, 331–346. doi:10.1016/j.neuroimage.2018.07.003.

de Schipper, L.J., Hafkemeijer, A., Bouts, M.J., van der Grond, J., Marinus, J., Henselmans, J.M., van Hilten, J.J., 2019. Age-and disease-related cerebral white matter changes in patients with parkinson's disease. Neurobiology of aging 80, 203–209.

Schmahmann, J., Pandya, D., 2006. Fiber pathways of the brain oxford university press. New York .

Scholz, J., Klein, M.C., Behrens, T.E., Johansen-Berg, H., 2009. Training induces changes in white-matter architecture. Nature neuroscience 12, 1370–1371.

Schüz, A., Braitenberg, V., 2002. The human cortical white matter: quantitative aspects of cortico-cortical long-range connectivity. Cortical areas: Unity and diversity , 377–385.

Setsompop, K., Gagoski, B.A., Polimeni, J.R., Witzel, T., Wedeen, V.J., Wald, L.L., 2012. Blipped-controlled aliasing in parallel imaging for simultaneous multislice echo planar imaging with reduced g-factor penalty. Magnetic resonance in medicine 67, 1210–1224.

Setsompop, K., Kimmlingen, R., Eberlein, E., Witzel, T., Cohen-Adad, J., McNab, J.A., Keil, B., Tisdall, M.D., Hoecht, P., Dietz, P., Cauley, S.F., Tountcheva, V., Matschl, V., Lenz, V.H., Heberlein, K., Potthast, A., Thein, H., Van Horn, J., Toga, A., Schmitt, F., Lehne, D., Rosen, B.R., Wedeen, V., Wald, L.L., 2013. Pushing the limits of in vivo diffusion mri for the human connectome project. Neuroimage 80, 220–33. doi:10.1016/j.neuroimage.2013.05.078.

Shastin, D., Chamberland, M., Parker, G., Tax, C.M.W., Koller, K., Hamandi, K., Gray, W., Jones, D., 2020. Delineating the grey matter-white matter interface directly from diffusion mri data, in: ISMRM, p. 4385.

Shastin, D., Rudrapatna, S.U., Parker, G., Hamandi, K., Gray, W., Jones, D., Chamberland, M., 2019. Tractography of complex white matter bundles: limitations of diffusion mri data upsampling, in: ISMRM, p. 3318.

Slater, D.A., Melie-Garcia, L., Preisig, M., Kherif, F., Lutti, A., Draganski, B., 2019. Evolution of white matter tract microstructure across the life span. Human brain mapping 40, 2252–2268.

Smith, R.E., Tournier, J.D., Calamante, F., Connelly, A., 2012. Anatomically-constrained tractography: improved diffusion mri streamlines tractography through effective use of anatomical information. Neuroimage 62, 1924–38. doi:10.1016/j.neuroimage.2012.06.005.

Smith, R.E., Tournier, J.D., Calamante, F., Connelly, A., 2015. Sift2: Enabling dense quantitative assessment of brain white matter connectivity using streamlines tractography. Neuroimage 119, 338–351.

Song, A.W., Chang, H.C., Petty, C., Guidon, A., Chen, N.K., 2014. Improved delineation of short cortical association fibers and gray/white matter boundary using whole-brain three-dimensional diffusion tensor imaging at submillimeter spatial resolution. Brain Connect 4, 636–40. doi:10.1089/brain.2014.0270.

St-Onge, E., Daducci, A., Girard, G., Descoteaux, M., 2018. Surface-enhanced tractography (set). Neuroimage 169, 524–539. doi:10.1016/j.neuroimage.2017.12.036.

Steinmetz, H., Fürst, G., Freund, H.J., 1989. Cerebral cortical localization: application and validation of the proportional grid system in mr imaging. Journal of computer assisted tomography 13, 10–19.

Stejskal, E.O., Tanner, J.E., 1965. Spin diffusion measurements: spin echoes in the presence of a time-dependent field gradient. The journal of chemical physics 42, 288–292.

Tournier, J.D., Calamante, F., Connelly, A., 2007. Robust determination of the fibre orientation distribution in diffusion mri: non-negativity constrained super-resolved spherical deconvolution. Neuroimage 35, 1459–72. doi:10.1016/j.neuroimage.2007.02.016.

Tournier, J.D., Calamante, F., Connelly, A., 2010. Improved probabilistic streamlines tractography by 2nd order integration over fibre orientation distributions, in: Proceedings of the international society for magnetic resonance in medicine, Ismrm.

Tournier, J.D., Smith, R., Raffelt, D., Tabbara, R., Dhollander, T., Pietsch, M., Christiaens, D., Jeurissen, B., Yeh, C.H., Connelly, A., 2019. Mrtrix3: A fast, flexible and open software framework for medical image processing and visualisation. NeuroImage , 116–137.

Van Essen, D.C., Jbabdi, S., Sotiropoulos, S.N., Chen, C., Dikranian, K., Coalson, T., Harwell, J., Behrens, T.E., Glasser, M.F., 2014. Mapping

connections in humans and non-human primates: aspirations and challenges for diffusion imaging, in: Diffusion MRI. Elsevier, pp. 337–358.

Vos, S.B., Aksoy, M., Han, Z., Holdsworth, S.J., Maclaren, J., Viergever, M.A., Leemans, A., Bammer, R., 2016. Trade-off between angular and spatial resolutions in in vivo fiber tractography. Neuroimage 129, 117–132. doi:10.1016/j.neuroimage.2016.01.011.

Vos, S.B., Tax, C.M., Luijten, P.R., Ourselin, S., Leemans, A., Froeling, M., 2017. The importance of correcting for signal drift in diffusion mri. Magn Reson Med 77, 285–299. doi:10.1002/mrm.26124.

Yeh, C.H., Smith, R.E., Dhollander, T., Calamante, F., Connelly, A., 2019. Connectomes from streamlines tractography: Assigning streamlines to brain parcellations is not trivial but highly consequential. Neuroimage 199, 160–171.

Zhang, F., Wu, Y., Norton, I., Rigolo, L., Rathi, Y., Makris, N., O'Donnell, L.J., 2018. An anatomically curated fiber clustering white matter atlas for consistent white matter tract parcellation across the lifespan. NeuroImage 179, 429–447.

Zhang, T., Chen, H., Guo, L., Li, K., Li, L., Zhang, S., Shen, D., Hu, X., Liu, T., 2014. Characterization of u-shape streamline fibers: Methods and applications. Medical image analysis 18, 795–807.

Zhang, Y., Zhang, J., Oishi, K., Faria, A.V., Jiang, H., Li, X., Akhter, K., Rosa-Neto, P., Pike, G.B., Evans, A., et al., 2010. Atlas-guided tract

reconstruction for automated and comprehensive examination of the white matter anatomy. Neuroimage 52, 1289–1301.